Inverse method to characterize "local" and "non-local" absorbing materials submitted to a shear grazing flow

Oleguer Berengue Llonch, Frank Simon, Estelle Piot
ONERA Centre de TOULOUSE, DMAE, France

Summary
As aircraft traffic is constantly increasing, serious efforts are made to find ways to reduce noise produced by the engines. Among them, the design of performing absorbing materials, called liners, placed on the nacelle's walls.ONERA has developed an "impedance" eduction method (code "Elvin") applied to materials with "local reaction" in the presence of shear grazing flow. The inverse process is based on wall acoustic pressure or velocity fields acquired by Laser Doppler Velocimetry (LDV) above the liner. Computations rely on the resolution of the 2D linearized Euler equations in the harmonic domain, spatially discretized by a discontinuous Galerkin scheme, which presents advantageous properties. First, it is weakly dispersive and dissipative. In addition, boundary conditions are imposed through fluxes, which is particularly robust and straightforward. The minimization of the objective function is achieved by the resolution, at each iteration on the liner impedance, of the direct and adjoint equations. After a description of the architecture and current features of Elvin code, configurations of "linear" and "non-linear" liners are tested with the corresponding impedance eduction method from data measured in Onera aeroacoustic bench (B2A) or NASA flow ducts. Values of objective function are analysed in the impedance map to evaluate standard deviation associated to identified impedance. Then, the procedure to extend the code to open-cell porous media instead of "local reaction" liners is shown. This implies the integration of a computation domain in which acoustic propagation equations are solved in the media. The objective is to extract the macroscopic parameters governing viscous dissipation of sound waves in porous media, from Biot theory or derived theories : open porosity, static flow resistivity, geometrical tortuosity, thermal and viscous characteristic dimensions... A first validation of direct equations is finally presented in impedance tube configuration (without flow) with implementation of Delany-Bazley's approach.

PACS no. 43.25.+y,43.50.+y

1. Introduction

Passive acoustic liners are classically arranged in engine nacelles to reduce the main contribution of external aircraft noise, ie the fan noise, in particular during the landing or take-off phase. These liners are generally porous "sandwich" resonators with a perforated plate linked to an honeycomb material above the rigid bottom. Their "local reaction" behavior can be described at first glance with the principle of an Helmholtz resonator. Nevertheless, the design of these kind of material must take into account the fact that the treatments are submitted to grazing turbulent high-speed flow (up to Mach 0.7) and high-pressure levels (140 to 160 dB). So, acoustic "vortices" of particle velocity can occur at the resonator surface generating a nonlinear dissipation mechanism (vortex shedding) and modifying the specific impedance. To reduce this effect, other solutions are studied like the using of "wire mesh" instead of perforated plate. Moreover, in order to enlarge the frequency range of absorption, different types of SDOF liners can be piled up to constitute 2DOF liners. However, their acoustic absorption ability is naturally limited to medium and high frequencies. To drastically improve their capabilities to the lowest frequencies (as needed for future Ultra High Bypass Ratio engines), the using of "non-local reaction" architectures (with foams, double-porosity elastic materials...) are of interest even if industrial application is yet tricky (ie. problems of fouling, robustness).

ONERA has developed an "impedance" eduction method (code "Elvin") applied to liner with "local reaction" in the presence of a grazing flow. The inverse process is based on wall acoustic pressure or velocity fields acquired by Laser Doppler Velocimetry (LDV) above the liner.The approach of identifying the impedance using data obtained by LDV has the advantage not to be intrusive and offers a larger amount of data than with an array of microphones.

Numerical simulations are made using a Discontinuous Galerkin (DG) method, see [4], well suited to solving direct and adjoint problems. applied to harmonic Linearized Euler equations.

This article will first describe the equations and the used numerical method (DG). The results will be presented with a confidence interval to bring up the limits and robustness of the method,through LDV measurements made by Onera and pressure data measured by NASA [5] and [6]).

Finally, an introduction to the extension of the code will be presented to open-cell porous media, in particular with a direct simulation of the acoustic propagation in both air and porous media.

2. Numerical method

2.1. Discontinuous Galerkin Formulation

The CAA solver relies on the computation of the 2-D harmonic Linearized Euler equations (LEEs) written with a time dependence $e^{j\omega t}$:

$$j\omega\varphi + \mathbf{A}^i\partial_i\varphi + \mathbf{B}\varphi = \mathbf{g} \tag{1}$$

with

$$\mathbf{A}_1 = \begin{pmatrix} U_0 & 0 & c_0 \\ 0 & U_0 & 0 \\ c_0 & 0 & U_0 \end{pmatrix},\ \mathbf{A}_2 = \begin{pmatrix} V_0 & 0 & 0 \\ 0 & V_0 & c_0 \\ 0 & c_0 & V_0 \end{pmatrix}$$

$$\text{and } \mathbf{B} = \begin{pmatrix} \partial_x U_0 & \partial_y U_0 & -\partial_x c_0 \\ \partial_x V_0 & \partial_y V_0 & -\partial_y c_0 \\ \frac{c_0}{\rho_0}\partial_x\rho_0 & \frac{c_0}{\rho_0}\partial_y\rho_0 & (\gamma-1)\left(\partial_x U_0 + \partial_y V_0\right) \end{pmatrix}$$

Where $\mathbf{g}$ is the source term and $\omega = 2\pi f$ the angular frequency. The vector $\varphi = \{u, v, c_0\rho/\rho_0\}^t$ represents the acoustic disturbances around the mean velocity (in 2 D U_0 and V_0); c_0 and ρ_0 are respectively the speed of sound and the density of the mean flow, and $c_0\frac{\rho}{\rho_0}$ is proportional to the acoustic pressure.

In addition, we can introduce the boundary conditions (matrix $\mathbf{M}$), and the connection between the elements:

$$\begin{cases} \mathbf{M}\varphi = 0 & \text{on the domain boundary} \\ \mathbf{A}^i n_i \varphi^* = 0 & \text{between the elements} \end{cases} \tag{2}$$

with $\overrightarrow{n}$ the normal vector in the output direction and φ^* the numerical flux, that will be defined afterwards.

Multiplying equations (1) and (2) by a test function ψ and integrating over a local open element ω_e belonging to the computational domain Ω with boundary $\partial\omega_e$ gives the weak formulation,

$$\begin{aligned} &\int_{\omega_e} \left(j\omega\varphi_e + \mathbf{A}^i\partial_i\varphi_e + \mathbf{B}\varphi_e\right).\psi_e d\omega_e \\ &\quad + \int_{\partial\omega_e\setminus\partial\Omega} \mathbf{A}^i n_i \varphi_e^*.\psi_e^- d\Gamma \\ &\quad + \int_{\partial\omega_e\cap\partial\Omega} \left(\mathbf{M}\varphi_e - \mathbf{g}\right).\psi_e d\Gamma = 0 \end{aligned} \tag{3}$$

where subscript e refers to the element ω_e. Furthermore, the fact that the solution and the test function can be discontinuous on the element edges let us introduce the definition of the interior and the exterior traces

$$\begin{cases} \psi_e^-(\mathbf{x}) = \lim\limits_{\mathbf{x}'\to\mathbf{x} \ and\ \mathbf{x}'\in\omega_e} \psi(\mathbf{x}') \\ \psi_e^+(\mathbf{x}) = \lim\limits_{\mathbf{x}'\to\mathbf{x} \ and\ \mathbf{x}'\notin\omega_e} \psi(\mathbf{x}') \end{cases} \tag{4}$$

idem for φ_e^- and φ_e^+ (figure 1).

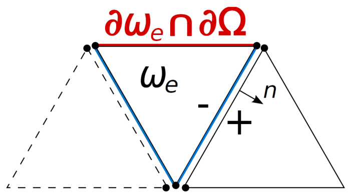

Figure 1. Element ω_e adjacent to the computational domain boundary

For the same reason, the numerical flux $\mathbf{A}^i n_i \varphi_e^*$ must be defined in order to impose the normal flux conservation across the element boundaries. A *upwind* scheme is chosen:

$$\varphi_e^* = \begin{cases} \varphi_e^- & \text{for outgoing waves} \\ \varphi_e^+ & \text{for ingoing waves} \end{cases} \tag{5}$$

In the presented method, a technique $flux-vector\ splitting$ (FVS) is used to fully exploit the hyperbolicity of the problem. As the matrix $\mathbf{A}^i n_i$ is diagonalizable, its eigenvectors are the phase speeds of the characteristics along the local normal vector. In addition, we can break it down into two matrices $\mathbf{A}^i n_i^+$ and $\mathbf{A}^i n_i^-$, respectively associated to its positive and negative eigenvalues:

$$\begin{aligned} \mathbf{A}^i n_i = \mathbf{P}\Lambda\mathbf{P}^{-1} &= \mathbf{P}\Lambda^+\mathbf{P}^{-1} + \mathbf{P}\Lambda^-\mathbf{P}^{-1} \\ &= \mathbf{A}^i n_i^+ + \mathbf{A}^i n_i^- \end{aligned} \tag{6}$$

This decomposition associated with the choice of a *upwind* scheme brings us to the next jump condition:

$$\mathbf{A}^i n_i^- \left(\varphi_e^+ - \varphi_e^-\right) = 0 \tag{7}$$

with

$$\mathbf{A}^i n_i^- = inf\,(u_n, 0) \begin{pmatrix} -\mathbf{n}\otimes\mathbf{n} & 0 \\ 0 & 0 \end{pmatrix} + \frac{u_n - c_0}{2} \begin{pmatrix} -\mathbf{n}\otimes\mathbf{n} & \mathbf{n} \\ \mathbf{n}^t & 1 \end{pmatrix} \quad (8)$$

where u_n is the acoustic velocity normal to the element boundary.

The weak formulation of the problem, after summation over the elements, is written as:

$$\int_{\omega_e} \left(j\omega\varphi_e + \mathbf{A}^i\partial_i\varphi_e + \mathbf{B}\varphi_e\right).\psi_e d\omega_e + \sum_e \int_{\partial\omega_e\setminus\partial\Omega} \mathbf{A}^i n_i^- \left(\varphi_e^+ - \varphi_e^-\right).\psi_e^- d\Gamma + \int_{\partial\omega_e\cap\partial\Omega} \left(\mathbf{M}\varphi_e - \mathbf{g}\right).\psi_e d\Gamma = 0 \quad (9)$$

Finally, projected over the local basis, the problem can be written as a system of linear equations

$$(j\omega\mathbf{N} + \mathbf{K})\,\Phi = 0 \quad (10)$$

where $\mathbf{N}$ and $\mathbf{K}$ are respectively the global mass and stiffness matrices.

2.2. Boundary Conditions

In order to avoid reflections at the open boundaries, we use the decomposition in incoming and outgoing waves. In this way, for a non-reflecting output condition, the matrix $\mathbf{M}$ is:

$$\mathbf{M} = -\mathbf{A}^i n_i^- \quad (11)$$

The source terms are also imposed with the same condition of non-reflection, that is to say,

$$\mathbf{M} = -\mathbf{A}^i n_i^- \; and \; \mathbf{g} = \varphi_{source} \quad (12)$$

Finaly, let $z = \frac{p}{\rho_0 c_0 v_n}$ be the reduced specific impedance, $\mathbf{M}$ can be expressed as a function of the reflection coefficient $\beta = \frac{z-1}{z+1}$):

$$\mathbf{M} = \frac{c_0}{2} \begin{pmatrix} (\beta+1)\,\mathbf{n}\otimes\mathbf{n} & (\beta-1)\,\mathbf{n} \\ -(\beta+1)\,\mathbf{n}^t & (1-\beta) \end{pmatrix} \quad (13)$$

This matrix $\mathbf{M}$ is used both for impedance boundary conditions and for the rigid wall boundary conditions expressed by $\beta = 1$.

2.3. Inverse method

The inverse method requires the minimization of the following objective function:

$$\Upsilon(\varphi, z, z_t, C) = \int_{\Omega_{obs}} \{\varphi\rfloor_{DG} - \varphi\rfloor_{Meas}\}^t . \{\varphi\rfloor_{DG} - \varphi\rfloor_{Meas}\}\, dxdy \quad (14)$$

where ω_{obs} is the measurement domain.

The BFGS-B algorithm (Broyden, Fletcher, Goldfarb, Shanno for bounded variables) is used to solve the optimization problem. The analytical formulation of gradients Υ relative to each parameter $z,\ z_t\ and\ C$ is obtained via the adjoint state.

$$\frac{\partial\Upsilon}{\partial z} = -\left\langle \frac{\partial\mathbf{M}_\beta}{\partial\beta}\frac{\partial\beta}{\partial z}\varphi, \varphi^{adj} \right\rangle_{\Gamma_l} \quad (15)$$

$$\frac{\partial\Upsilon}{\partial z_t} = -\left\langle \frac{\partial\mathbf{M}_{\beta_t}}{\partial\beta_t}\frac{\partial\beta_t}{\partial z_t}\varphi, \varphi^{adj} \right\rangle_{\Gamma_t} \quad (16)$$

$$\frac{\partial\Upsilon}{\partial C} = \left\langle \mathbf{A}^i n_i^- \varphi_0, \varphi^{adj} \right\rangle_{\Gamma_s} \quad (17)$$

where φ^{adj} is the solution of adjoint problem, and Γ_l, Γ_t Γ_s are respectively the liner, output and source surfaces.

3. Analysis of results

The inverse method described above will be used to calculate the impedance of a liner-type *wiremesh*. The used data come from the NASA GFIT bench ([5] and [6]) for which a large number of measurements (31 microphones) provides a rapid convergence to a suitable value.

The method was used for the case without flow (figure 3) and with flow at $M_C = 0.3$ (Figure 4), both with a $SPL = 130\ dB$. The results of the optimization are then processed to obtain a map of objective function.

A confidence interval of impedance to assess the robustness of the identification procedure is found for a reduced objective function (see eq. 19) lower than the desired threshold value, that is to say

$$Find \quad z = \theta + j\chi \quad for \quad \Upsilon_{red} \leqslant \kappa \quad (18)$$

where θ is the resistance, χ the reactance and κ the desired threshold value and with,

$$\Upsilon_{red} = \frac{\Upsilon}{\sum_{m=1}^{N} \parallel p_{meas}^m \parallel^2} \quad (19)$$

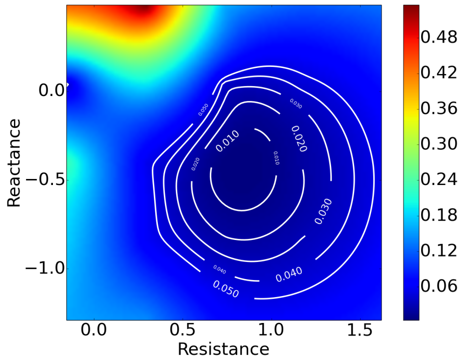

Figure 2. Objective function in the impedance plane for f=1600 Hz and $M_c = 0$

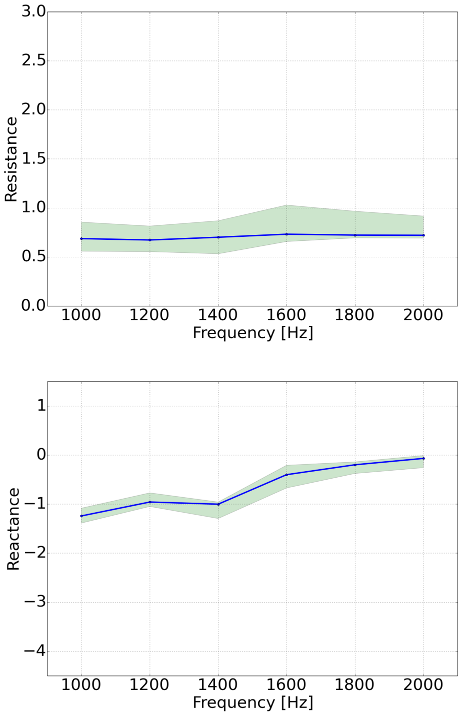

Figure 3. Results of impedance eduction of wiremesh liner with NASA pressure measurements. $M_c = 0$

The figure (2) is an example of objective function represented in the impedance plane at a given frequency for $\kappa = 0.01$.

Figure 3 shows the impedance eduction results for the case without flow with the confidence interval (green colored surface) corresponding to the possible values of θ (or χ) to have a value of the cost function lower than κ. One can notice that the confidence interval has a similar size for all the studied frequencies. This means that the sensitivity of identification is the same for all cases.

We can see now in figure 4, corresponding to the case with flow $M = 0.3$, a frequency, that is to say 1400 Hz, for which the confidence interval is reduced, sign of an accurate identification of impedance.

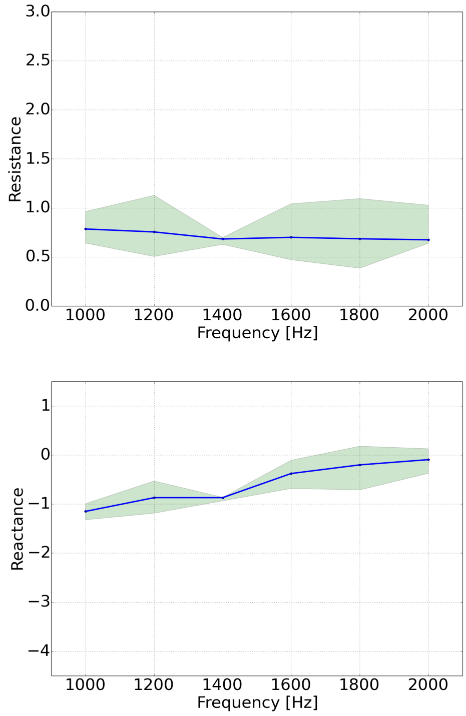

Figure 4. Results of impedance eduction of wiremesh liner with NASA pressure measurements. $M_c = 0.3$

We then study the case of a conventional liner with non-linear behavior obtained by a micro-perforated plate, characterized by LDV measurements in the Onera B2A bench [5]. In this way, we can test the robustness of the code not only for pressure measurements, but also for the measurement of velocity field above a liner.

The results of the identification of the impedance without flow (Figure 5) and with shear flow of $Mc = 0.23$ (figure 6) show results more robust than in the case of identification with microphones. It can be explained by the high number of measurement points (300 points of acoustic velocity) in 2 directions and close to the liner.

Moreover, at high frequencies, the confidence interval is lower than at low frequencies, thus ensuring a more accurate identification.

4. Extension to porous media

The impedance eduction method can be extended to the case of porous materials. This requires a computational domain in which the equations of acoustic propagation in porous materials are resolved. The objective therefore is to identify parameters representative of the acoustic absorption of a porous material : the flow resistance, porosity, etc.

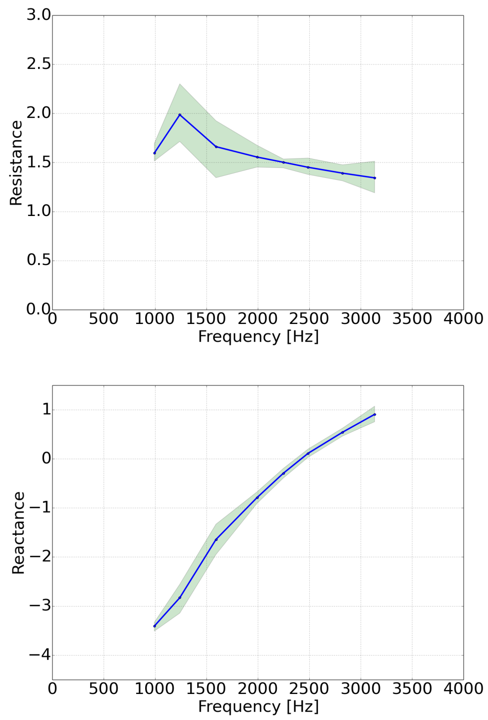

Figure 5. Results of impedance eduction of micro-perforated liner with Onera LDV measurements. $M_c = 0$

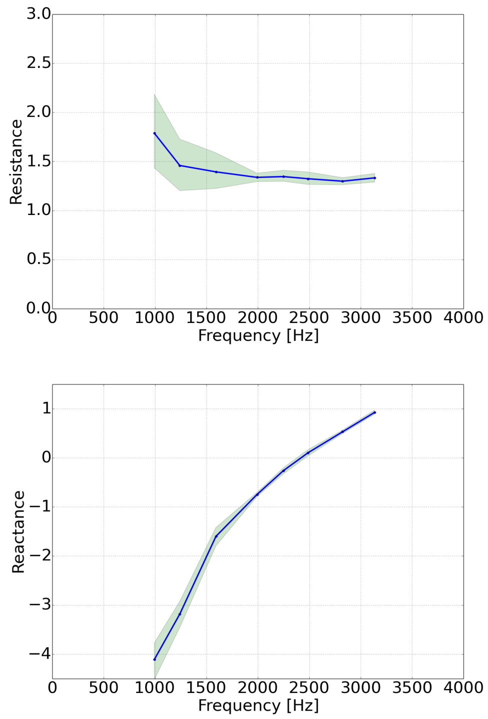

Figure 6. Results of impedance eduction of micro-perforated liner with Onera LDV measurements. $M_c = 0.23$

4.1. Discontinuous Galerkin for the coupling air-material

Discontinuous Galerkin method has been established for the 1D problems, such as an impedance tube. The method uses generalized Biot equations to solve the acoustics within the material, as well as air-material coupling conditions for propagating waves at the interface.

Generalized Biot's equations can be written as:

$$\mathbf{A}\partial\varphi + \mathbf{B}\varphi = \mathbf{g} \tag{20}$$

with

$$\mathbf{A} = \begin{pmatrix} k_b + \frac{4}{3}N & 0 & 0 & 0 \\ 0 & 1 & 0 & 0 \\ 0 & 0 & 0 & 1 \\ 0 & 0 & 1 & 0 \end{pmatrix}$$

and $\mathbf{B} = \begin{pmatrix} 0 & \tilde{\gamma} & \tilde{\rho}\omega^2 & 0 \\ \frac{\tilde{\rho_e}}{\phi}\tilde{\gamma}\omega^2 & 0 & 0 & \frac{\tilde{\rho_e}}{\tilde{k}f}\omega^2 \\ 0 & -1 & 0 & 0 \\ -1 & 0 & 0 & 0 \end{pmatrix}$

where all the parameters used in these matrices are described in [1] and the state vector is $\varphi = \{\partial_x u, \partial_x p, u, p\}^t$.

With this matrix formulation, we can find the following weak formulation:

$$\begin{aligned} &\int_{\omega_e} \left(\mathbf{A}\partial_i\varphi_e + \mathbf{B}\varphi_e\right).\psi_e d\omega_e \\ &+ \sum_e \int_{\partial\omega_e\backslash\partial\Omega} \mathbf{K}n\left(\varphi_e^+ - \varphi_e^-\right).\psi_e^- d\Gamma \\ &+ \int_{\partial\omega_e\cap\partial\Omega} \left(\mathbf{M}\varphi_e - \mathbf{g}\right).\psi_e d\Gamma = 0 \end{aligned} \tag{21}$$

where $\mathbf{K}$ is the numeric flux between two cells of the mesh and $\mathbf{M}$ the boundary conditions.

In this case we can use the following numeric flux:

$$\varphi^* = \left\{ \begin{array}{c} \{\{\partial_x u\}\} - \tau_1 [[u]] \\ \{\{\partial_x p\}\} - \tau_2 [[p]] \\ \{\{u\}\} \\ \{\{p\}\} \end{array} \right\} \tag{22}$$

We obtain the matrix $\mathbf{K}$ such that:

$$\mathbf{K} = \frac{1}{2}\begin{pmatrix} k_b + \frac{4}{3}N & 0 & 2\tau_1\left(k_b + \frac{4}{3}N\right)\mathbf{n} & 0 \\ 0 & 1 & 0 & 2\tau_2\mathbf{n} \\ 0 & 0 & 0 & 1 \\ 0 & 0 & 1 & 0 \end{pmatrix}$$

For rigid wall boundary conditions, we can consider the same approach as for the linearized Euler equations, that is to say:

$$\mathbf{M} = \frac{\mathbf{n}}{2}\begin{pmatrix} 0 & 0 & -2\tau_1\left(k_b + \frac{4}{3}N\right)\mathbf{n} & 0 \\ 0 & -2 & 0 & 0 \\ 0 & \frac{2j\mathbf{n}}{\tilde{\rho_e}\omega} & 0 & 0 \\ 0 & 0 & -1 & 0 \end{pmatrix}$$

Finally, the conditions at the air-material interface is the continuity of pressure and displacement eq. (23):

Table I. Characteristics of melamine foam

Thickness d $[m]$	0.04
Porosity ϕ	0.99
Flow resistivity σ $[Nm^{-4}s]$	12000
Viscous Dimension Λ $[\mu m]$	100
Thermic Dimension Λ' $[\mu m]$	400
Tortuosity α_∞	1.01
Density ρ_1 $[kgm^{-3}]$	9
Shear modulus N $[kPa]$	86
Poisson coefficient ν	0.276
Damping η	0.75

$$\begin{aligned} p^{air} &= p^{mat} \\ \partial_x p^{air} &= \rho_{air}\omega^2(1-\phi-\phi\frac{\tilde{\rho_{12}}}{\tilde{\rho_{22}}})u^{mat} \\ &+\frac{\phi\rho_{air}}{\tilde{\rho_e}}\partial_x p^{mat} \end{aligned} \tag{23}$$

The next step will be, as for "impedance" eduction method, to formulate an inverse method, called "Biot parameters" eduction method, to identify parameters characteristic of the material, from acoustic pressure or velocity experimental data (see eq. (14)).

4.2. Results

The absorption coefficient of a melamine foam (see Table I) was computed in frequency, assuming the propagation of plane waves and determining the acoustic pressure at two points, as in impedance tube [2]. The results are then compared with a model type Delany-Bazley [3] (see Figure 7).

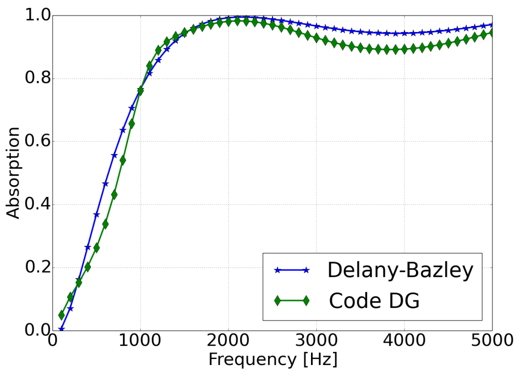

Figure 7. Absorption coefficient with Delany-Bazley model and Onera code

One can notice a good agreement between the results of the semi-empirical model of Delany-Bazley and the numerical results of the developed code, which is satisfying for the future "Biot parameters" eduction method.

5. CONCLUSIONS

A study of the robustness of the Onera code of impedance eduction was made for different cases of grazing flow, a liner with a "wiremesh", from data provided by NASA, and a conventional "microperforated" liner, from data provided by Onera. For the first type of material, we obtained a frequency confidence interval, giving us an estimate of the robustness of the code with an array of microphones. For the second case of material, the confidence interval using LDV measurements is much smaller than that obtained for wiremesh with pressure measurements. This leads us to conclude that, if we want to minimize the sensitivity of the eduction result, it will be appropriate to use LDV measurements. Finally, a proposal to extend the eduction code to porous materials was presented: that is to say, the weak formulation of the problem, the numerical flux and the boundary conditions. A first validation in a 1D case has been made by comparison with results provided by the semi-empirical model type Delany-Bazley. The implementation of porous materials in the developed code "Elvin" will continue in duct with grazing flow.

References

[1] M.A. Biot: The theory of propagation of elastic waves in a fluid-saturated porous solid. i. low frequency. ii. higher frequency range. JASA 28 (1956) 168-191.

[2] H. Boden, M. Abom: Influence of errors on the microphone method for measuring acoustics properties in ducts. JASA 79(2) (1986) 541-549.

[3] M. E. Delany, E. N. Bazley: Acoustical properties of fibrous absorbent materials. Applied Acoustics 3 (1970)105-116.

[4] J. Primus: An adjoint-base method for liner impedance eduction: Validation and numerical investigation. JSV, Vol. 332, No. 1 (2013) 58-75.

[5] J. Primus, E. Piot, F. Simon, M. G. Jones, W. R. Watson: ONERA-NASA Cooperation Effort on Liner Impedance Eduction. Proc.19th AIAA/CEAS Aeroacoustics Conference, no 2013-2273, AIAA (2013).

[6] M. G. Jones, W. R. Watson: On the use of experimental methods to improve confidence in educed impedance. Proc. 17th AIAA/CEAS Aeroacoustics Conference, no 2011-2865, AIAA (2011).